Microporous and Mesoporous Materials 122 (2009) 208–215

Contents lists available at ScienceDirect

Microporous and Mesoporous Materials

journal homepage: www.elsevier.com/locate/micromeso

Characterization of Sn- and Zn-loaded MCM-41 catalysts for nopol synthesis

Edwin A. Alarcón, Aída Luz Villa *, Consuelo Montes de Correa

Environmental Catalysis Research Group, Universidad de Antioquia, SIU, Cra. 53, N° 61-30, Medellín, Colombia

ARTICLE INFO

Article history:
Received 22 May 2008
Received in revised form 29 December 2008
Accepted 2 March 2009
Available online 11 March 2009

Keywords:
Nopol
Sn–MCM-41
Zn–MCM-41
CVD
Hydrothermal synthesis

ABSTRACT

Several heterogeneous catalysts based on MCM-41 were synthesized either by chemical vapor deposition (CVD) or hydrothermally, i.e. adding $SnCl_4$, $SnCl_2$ or $ZnCl_2$ as precursor salts into the MCM-41 synthesis gel. Synthesized materials were characterized by XRD, BET surface area, atomic absorption, UV–Vis, H_2-TPR, NH_3-TPD, TEM and pyridine-FTIR. Better textural properties and more reactive materials were obtained using tin salt precursors compared with $ZnCl_2$. UV–Vis and TPR analyses of selected Sn–MCM-41 materials indicate that depending on the synthesis and pretreatment conditions several species may be formed: Sn^{4+} as Lewis acid sites of different coordination, SnO_2 nanoparticles and bulk tin oxide species. The presence of SnO_2 nanoparticles was also confirmed by TEM. Medium strength Lewis acid sites appear to increase nopol selectivity. Hydroxylated groups, i.e. Sn–OH, increased the weak acid sites and diminished nopol selectivity.

1. Introduction

Nopol is an important starting material for the synthesis of fragrances and household products [1]. Quantitative nopol yields larger than 95% based on paraformaldehyde, and 86% nopol selectivities based on β-pinene are typically obtained at 180 °C [2]. On the other hand, by using homogeneous catalysts such as $ZnCl_2$, nopol yields are about 71% between 105 and 120 °C [3,4]. We have recently found that Sn–MCM-41 materials are promising heterogeneous catalysts for the Prins condensation of β-pinene and paraformaldehyde at 90 °C. Corma et al. also evaluated several Sn–MCM-41 catalysts synthesized under hydrothermal conditions at 135 °C [5,6]. More recently, Zn–Al–MCM-41 [7] and mesoporous iron phosphate [8] were reported for nopol production. Typically, nopol yields above 80% have been obtained over the above heterogeneous catalysts under mild reaction conditions.

Although, high nopol yields have been obtained over Sn–MCM-41 prepared by chemical vapor deposition (CVD) of $SnCl_4$, several steps are required for obtaining these materials. Besides, $SnCl_4$ is hazardous and must be handled carefully under inert atmosphere because it hydrolyzes in air. Alternatively, $SnCl_2$ has been used as Sn precursor and is easier to handle [9–11]. In this contribution, several Sn–MCM-41 synthesis procedures are assessed for nopol production. Additionally, Zn-loaded materials were hydrothermally synthesized at room temperature using $ZnCl_2$ as precursor salt. Selected materials were characterized by XRD, single point BET surface area, atomic absorption, UV–Vis, TEM, H_2-TPR, NH_3-TPD, pyridine-FTIR and tested for the Prins condensation of β-pinene and paraformaldehyde to obtain nopol.

2. Experimental

2.1. Materials

Commercial products were used as received: myristyltrimethylammonium bromide ($CH_3(CH_2)_{13}N(Br)(CH_3)_3$, 99 wt%, Aldrich), tetra ethyl ortho silicate (TEOS 98 wt%, Acros Organics), aqueous ammonia (28–30 wt%, EM Science), anhydrous $SnCl_4$ (99.995 wt%, Aldrich), $SnCl_2 \cdot 2H_2O$ (reagent grade, AlfaAesar), $ZnCl_2$ (reagent grade, Merck), β-pinene (99 wt%, Aldrich), paraformaldehyde (95 wt%, Aldrich), toluene (99.5 wt%, Mallinckrodt) and anhydrous dodecane (99 wt%, Aldrich).

2.2. Catalyst synthesis

MCM-41 was synthesized following the procedure reported by Grün et al. [12]. Myristyltrimethylammonium bromide was used as template and $SnCl_4$, $SnCl_2 \cdot 2H_2O$ and $ZnCl_2$ as metal precursors of Sn- or Zn-loaded materials. CVD was carried out by batch and continuous processes and resulting catalysts coded $SnMB_x$, $SnMC_x$, $ZnMC_x$, where, B and C correspond to batch and continuous processes, respectively and x to the metal loading in μmol/g as determined by atomic absorption. In a typical synthesis of $SnMB_x$ materials [5], calcined MCM-41 (0.5 g) was exposed to the vapors generated by $SnCl_4$ (10–160 μmol) at 100 °C for 8 h. SnMNCB0 (Table 1, entry 6) was prepared by CVD of $SnCl_4$ over as synthesized MCM-41 following a previous reported procedure [13]. $SnMC_x$

* Corresponding author. Tel.: +57 4 2198535; fax: +57 4 2196609.
E-mail address: alvilla@udea.edu.co (A.L. Villa).

1387-1811/$ - see front matter © 2009 Elsevier Inc. All rights reserved.
doi:10.1016/j.micromeso.2009.03.003

Table 1
Metal loading and BET surface area of Sn- and Zn-loaded MCM-41 materials.

Entry	Catalyst[a]	Metal precursor	μmol Me/g support[b]	% metal Deposition	BET Surface area(m^2/g)
1	SnMB70[c]	$SnCl_4$	320	21.9	nd
2	SnMB16	$SnCl_4$	160	9.8	1106 ± 6
3	SnMB25	$SnCl_4$	80	30.7	963 ± 60
4	SnMB7	$SnCl_4$	40	17.5	1049 ± 40
5	SnMB0	$SnCl_4$	20	< 0.2	984 ± 30
6	SnMNCB0[d]	$SnCl_4$	80	< 0.06	1075 ± 6
7	M0	None	0	0	929 ± 29
8	SnMC113	$SnCl_2{\cdot}2H_2O$	320	35.2	963 ± 16
9	SnMC68	$SnCl_2{\cdot}2H_2O$	160	42.2	1154±21
10	SnMC129[e]	$SnCl_2{\cdot}2H_2O$	320	40.4	1072 ± 19
11	ZnMC174	$ZnCl_2$	320	54.5	nd
12	ZnMC118	$ZnCl_2$	160	73.6	816 ± 14
13	SnMG195	$SnCl_4$	446[f]	43.7	976 ± 188
14	SnMG135	$SnCl_2{\cdot}2H_2O$	446[f]	30.3	980 ± 23
15	SnMG94	$SnCl_2{\cdot}2H_2O$	223[f]	42.2	1069 ± 1
16	ZnMG340	$ZnCl_2$	446[f]	76.2	478 ± 67
17	ZnMG142	$ZnCl_2$	223[f]	63.7	600 ± 5

nd: Not determined.
[a] The numbers in catalyst codes indicate the μmol metal loading/g catalyst determined by atomic absorption.
[b] μmol metal loading/g catalyst employed in the synthesis gel.
[c] Corresponds to the catalyst Sn-MCM-41-D2 cited in Table 2 of reference [5].
[d] The support was as synthesized MCM-41.
[e] Material synthesized using 25 mL/min of flowing gases.
[f] Assuming the amount of SiO_2 in the synthesis gel of MCM-41.

and $ZnMC_x$ materials (Table 1, entries 8–12) were obtained by CVD of $SnCl_2$ or $ZnCl_2$ on calcined MCM-41 in a tubular reactor at 450 or 500 °C, respectively, under a stream of 25–50 ml/min N_2. The recovered solids were washed with deionized water until negative chloride test and dried at 100 °C. $SnMG_x$ and $ZnMG_x$ materials were hydrothermally synthesized following a reported procedure by Stockenhuber et al. [14]. In a typical synthesis, aqueous ammonium hydroxide (2.0 ml) was added into a solution of myristyltrimethylammonium bromide (0.74 g) and deionized water (32.6 ml). The initial pH of the homogeneous solution was measured with an Orion 3 Star pH meter equipped with a glass electrode 9272BN. Then, $SnCl_2 \cdot 2H_2O$ or $ZnCl_2$ (180–360 μmol) was added followed by drop wise addition of TEOS (2.8 g). The resulting mixture was stirred 1 h at room temperature. The gel composition was SiO_2:xMeO$_y$:0.152MTABr:2.8NH_4OH:141·$2H_2O$, where MeO$_y$ corresponds to SnO_2 or ZnO and x to 0.0268 or 0.0134. The resulting solids were filtered, washed with deionized water until negative chloride test, dried at 100 °C for 12 h and calcined at 550 °C for 5 h (entries 13–17).

2.3. Characterization

XRD analyses were carried out in an AXS Brucker diffractometer with copper radiation. Atomic absorption was performed in a Thermo Elemental SOLAAR S4 Spectrometer. BET surface area was determined by single BET point measurement in a Micromeritics Autochem 2920; before nitrogen adsorption (5% N_2/He) the sample was degassed at 150 °C for 30 min. UV–Vis spectra were recorded in a Shimadzu Spectrophotometer using barium sulfate as reference. TEM micrographs were obtained in a Hitachi 200 kV instrument. Temperature programmed desorption of ammonia (TPDA) was carried out in a Micromeritics Autochem 2920 instrument. Typically, a 0.05 g sample was heated at 10 °C/min in flowing 50 ml/min He up to 550 °C for 30 min. Then, the sample was cooled at 40 °C and saturated with 50 ml/min of 0.3% NH_3/He during 1.5 h. Physisorbed ammonia was flushed with 25 ml/min He at 40 °C for 1 h. Finally, ammonia was desorbed by increasing the temperature up to 800 °C at 10 °C/min in flowing helium. The TCD signal was calibrated with ammonia mixtures of known composition. Blank experiments were carried out over the support using helium instead of ammonia. Signal deconvolution was carried out with Microcal Origin 6.0. Temperature programmed reduction (TPR) measurements were performed in a Micromeritics Autochem 2920 instrument. The samples were pretreated following the same procedure used in TPDA analysis and reduced in 25 ml/min of flowing 5% H_2/Ar from room temperature to 1100 °C at 10 °C/min. Two blank experiments were performed: with no sample (blank 1) and by flowing pure Ar through a sample (blank 2). For FTIR-pyridine analysis, catalyst samples were previously activated at 200 °C under vacuum for 24 h and stored for 24 h at room temperature in a closed vessel under the vapors generated from water-free pyridine. FTIR spectra at room temperature were obtained in a Perkin–Elmer Spectrum 1 FTIR using 32 scans with a resolution of 4 cm^{-1}.

2.4. Catalytic tests

Reactions were performed in 2 ml vials immersed in an oil bath at 90 °C. Both the oil bath and vial mixtures were homogenized by magnetic stirring. The reactions were carried out at 90 °C for 1 h using mixtures of paraformaldehyde (0.5 mmol), toluene (0.5 ml), β-pinene (0.25 mmol) and 25 mg catalyst samples. The reaction products were identified by gas chromatography using a Varian Star 3400 equipped with a flame ionization detector (FID), a CP 8200 autosampler and a DB-1 capillary column (0.32 mm × 50 m × 1.20 μm). The oven temperature was increased from 140 to 195 °C. The quantification of nopol and β-pinene was carried out with multi point calibration curves using dodecane as internal standard. Response factors were determined from the curve slopes. Conversion and selectivity were determined according to Eqs. (1) and (2)

$$\%\ \text{Conversion} = \frac{(C_{ti} - C_{tf})_{\beta-\text{pinene}}}{(C_{ti})_{\beta-\text{pinene}}} 100\% \quad (1)$$

$$\%\ \text{Selectivity} = \frac{(C_{tf})_{\text{nopol}}}{(C_{ti} - C_{tf})_{\beta-\text{pinene}}} 100\% \quad (2)$$

where C_{ti} and C_{tf} are the initial and final concentrations.

2.5. Leaching tests

Leaching tests were carried out according to reported procedures [15]. In a typical reaction a 6 mg catalyst sample was added to a mixture (kept at 90 °C) of 1 ml of 0.5 M β-pinene in toluene, and a paraformaldehyde: β-pinene ratio of 2:1. The catalyst was removed from the reaction mixture when conversions were lower than 20% (5 min reaction time) and the filtrate analyzed for further reactions. Then, paraformaldehyde was added to the filtrate and stirring continued at 90 °C for 3, 6 and 24 h. A blank reaction was carried out under the same conditions of the leaching tests but, with no catalyst.

3. Results and discussion

3.1. Elemental analysis, XRD diffraction, BET

As can be observed in table 1 Sn was more efficiently deposited by CVD when $SnCl_2 \cdot 2H_2O$ was used as metal source as compared to $SnCl_4$ (entries 1–6 and 8–10), probably because of the higher temperature used with the stannous precursor. No Sn was detected in SnMNCB0 (entry 6) [13]. It might suggest that the anchoring sites within the channels of MCM-41 are fundamental for Sn deposition. Under the same synthesis conditions, Zn was more efficiently deposited than Sn (entries 9 and 12). A slight increase of deposited tin was obtained when the gas flow was reduced to a half (entries 8 and 10). The Sn loading increased when the amount of $SnCl_2$ precursor decreased, either by CVD (entries 8 and 9) or by hydrothermal procedures (entries 14 and 15). Larger Sn loadings on hydrothermally synthesized Sn–MCM-41 were obtained with $SnCl_4$ as precursor (entries 13 and 14) compared to $SnCl_2$, more likely because $SnCl_4$ rapidly hydrolyzed.

BET surface areas of Sn–MCM-41 materials varied between 929 and 1154 m^2/g and did not depend on the synthesis method. Zn modified materials exhibited lower surface areas than Sn-loaded materials particularly those synthesized by hydrothermal method. Sn–MCM-41 samples synthesized by CVD of $SnCl_4$ showed the characteristic XRD features of MCM-41 materials (see Fig. 1a). A strong peak at 2.6° (d_{100} = 33.19 Å), and two smaller reflection peaks at 4.6° (d_{110} = 19.06 Å) and 5.4° (d_{200} = 16.43 Å) are typical of hexagonal channels. Also a peak around 7° (d_{210} = 12.63 Å) can be observed. No significant *d*-spacing displacement was observed after $SnCl_4$ deposition. More ordered materials were obtained upon additional heat treatment since the intensity of the main peak increased with respect to the support, M0. Because of the pretreatment conditions, i.e. high temperatures and very reactive acid precursors, the intensity of the characteristic MCM-41 peaks decreased when $SnCl_2$ or $ZnCl_2$ were used as precursors in the CVD method, Fig. 1b, and is attributed either to depolymerization of silica walls [17] or to hexagonal symmetry decrease [18]. The low intensity and peak broadening observed in the XRD pattern of Zn-loaded catalysts indicate that these materials are not well ordered [16], i.e. the hexagonal array of their channels is not quite regular. The high temperature required to deposit $ZnCl_2$ and $SnCl_2 \cdot H_2O$ by CVD may be responsible for high metal loading and diminished hexagonal geometry of the resulting materials, mainly those prepared using $ZnCl_2$ as precursor. XRD of SnMG195 (not shown) only exhibited the main peak moreover SnMG94 displayed both 110 and 200 reflections. Although, SnMG135 exhibited a surface area similar to Sn–MCM-41, its diffraction pattern did not correspond to an organized structure (not shown). The d_{100} reflections in the XRD patterns of Zn-loaded materials synthesized by CVD shifted to lower d-spacing. Sn–MCM-41 materials prepared by hydrothermal method at room temperature appear to be an alternative option. Zn-loaded materials hydrothermally synthesized did not show the characteristic peaks of MCM-41 [19], although, Zn/Si ratios lower than 0.1 were used as suggested by Kowalak and co-workers [20]. Since Zn-loaded materials with hexagonally ordered channels were not obtained by this methodology, other synthesis variables should be considered in future studies.

3.2. TPR-H_2

TPR-H_2 was carried out to determine reducible species in synthesized materials. Signals corrected with blank experiments are displayed in Fig. 2. As shown in Fig. 2, the reduction peaks at 690

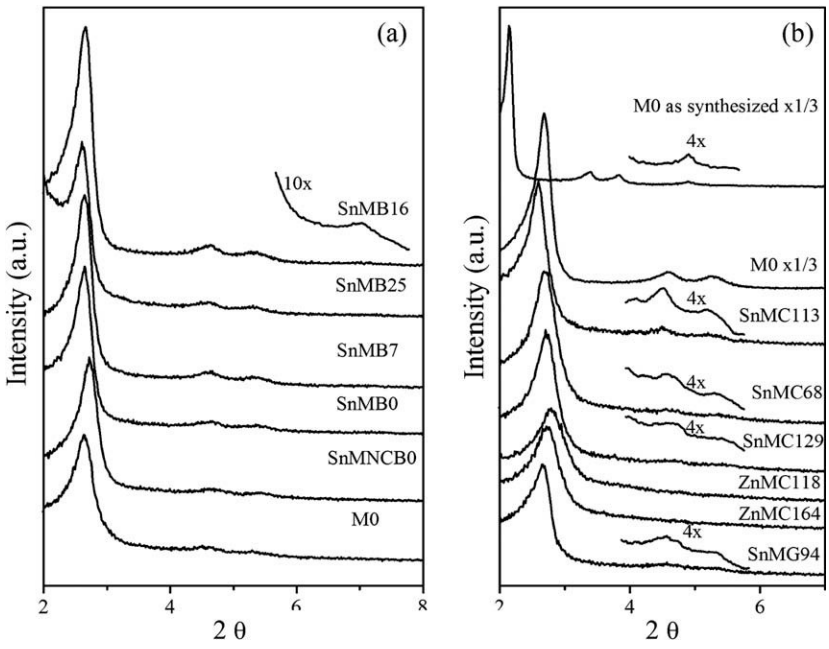

Fig. 1. (a) XRD patterns of synthesized materials by CVD of $SnCl_4$, and (b) hydrothermally synthesized using $SnCl_2$ or $ZnCl_2$ as precursors.

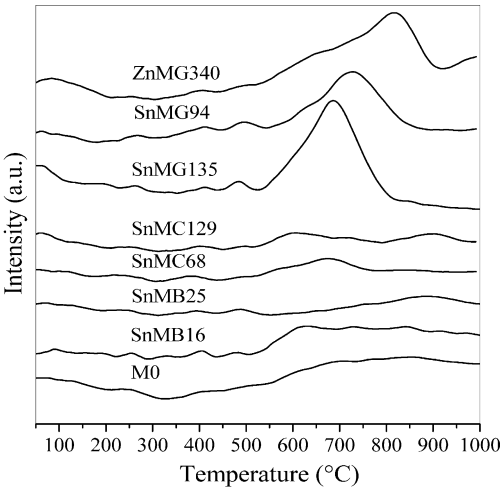

Fig. 2. H_2-TPR profiles of several Sn-loaded MCM-41 materials.

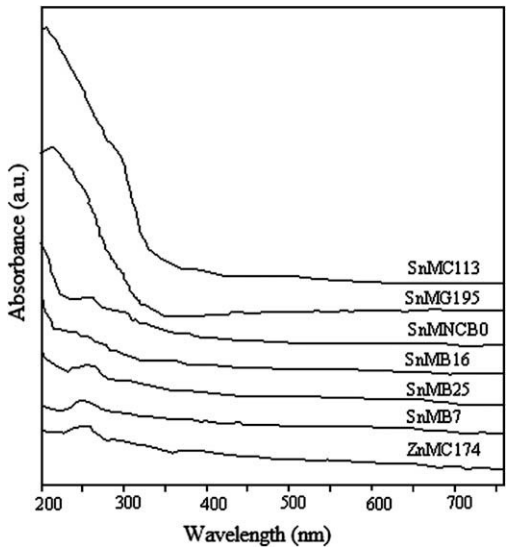

Fig. 3. UV–Vis spectra of several Sn- and Zn-loaded MCM-41 materials.

and 730 °C for SnMG135 and SnMG94, respectively, have been attributed to the presence of bulk tin oxide species (SnO_x) [21,22]. Reduction peaks below 600 °C are assigned to isolated sites of tin oxide nanoparticles or nanofilms of Sn–MCM-41 [21]. The broad peak at 810 °C with shoulders at lower temperatures in the ZnMG340 profile might be attributed to reducible ZnO species of different sizes [23]. In spite of the high Sn and Zn loadings of CVD materials no characteristic signals of reducible species were observed. Therefore, the metal environment of materials prepared by CVD is quite different from that of materials prepared by direct hydrothermal synthesis at room temperature.

Under basic conditions, i.e. SnMG, it has been suggested that insoluble $Sn(OH)_4$ species [24], α-stannic acid, or hydrous tin (IV) oxide ($SnO_2 \cdot H_2O$) [25] are formed after aqueous ammonia hydrolysis [26,27]. Besides, co-precipitation of Sn with silicon species produces dispersed tin sites or stannic acid aggregates that could be occluded into MCM-41 channels. SnO_x agglomerates are formed after heat treatment in oxygen, which is in agreement with TPR-H_2 measurements (Fig. 2). Furthermore, stannous chloride could generate complexes with water and ammonia that are transformed into tin oxide species after calcination [25]. On the other hand, it is well known that silanol groups play an important role for anchoring the reactive precursor; it has been suggested that Sn–OH and Sn–O–Sn species are produced after grafting organotin chloride compounds and tin tetrachloride, respectively [28,29].

3.3. UV–Vis and TEM

Fig. 3 shows the UV–Vis spectra of selected materials. The intensity of the characteristic bands of Sn–MCM-41 varied with tin loading. The spectra of $SnMB_x$ materials are not well defined probably because of their low tin loading; however, one of the characteristic signals is observed around 243 nm suggesting the presence of highly dispersed tetrahedral isolated Sn^{4+}, ascribed to charge transition from O_2^- to Sn^{4+} in a tetrahedral coordination environment. SnMG195 and SnMC113 show a broad band around 208 nm suggesting the presence of Sn^{4+} in tetrahedral coordination in the silica framework [19]. Site-isolated Sn in a distorted tetrahedral environment and/or in penta- or octahedral coordination sphere may be associated with such broadening character of SnMG195 and SnMC113 spectra. It was suggested that the amorphous nature of the pore wall having wide range of Sn–O–Si bond angles might cause the distortion in tetrahedral environment of Sn species and hydration of some of the Sn sites might result in the formation of Sn sites with coordination number higher than four [30]. This broad band may overlap signals around 230 and 280 nm. It was reported that pure SnO_2 exhibited a broad absorption at ~280 nm assigned to hexacoordinated polymeric Sn–O–Sn type species [20]. A blue shift of the absorption edge in comparison to bulk SnO_2 (absorption at ~280 nm) in the spectra of Sn-loaded samples is observed in Fig. 3. These blue shifts result from the size-quantization effect and indicate SnO_2 particles in the nanometer regime [31]. The UV–Vis band around 280 nm in the spectrum of ZnMC174 may be assigned to ZnO encapsulated nanoparticles [32–34]. The spectrum of ZnMG340 (not shown) does not display any band.

In Fig. 4 TEM micrographs of SnMB25 show the hexagonal structure of MCM-41 type materials, in agreement with the XRD data. Also the solid seems homogeneous as if the tin atoms had been deposited uniformly. However, most of the pores appear grey indicating an increase of the electron density in the interior and, thus, the presence of Sn oxide species [31]. It is highly probable that in the wide pores of the MCM-41 structure aggregates consisting of several Sn atoms formed.

3.4. NH_3-TPD

The acid nature of several Sn– and Zn–MCM-41 materials was evaluated by temperature programmed desorption of ammonia (TPDA). The TPDA profile has been divided into two regions according to the acid strength; a low temperature region ($T < 400$ °C) related to weak acid sites and a high temperature region ($\geqslant 400$ °C) attributed to strong acid sites [35]. According to ammonia desorption energy measurements, weak, medium and strong acidity have been also assigned to signals in the 180–250, 280–330 and 380–500 °C region, respectively [36]. Signals below 180 °C are usually assigned to ammonia physisorption on very weak acid sites [37]. Blank experiments (not shown) exhibited a broad desorption band starting around 550 °C, which has been associated with dehydroxylation of silanol groups [17].

As can be observed in table 2 and Fig. 5 all analyzed materials exhibited three main signals. Zn-loaded materials exhibited higher amount of acid sites than Sn–MCM-41. Although, total acidity is not directly related to metal loading, materials with low metal contents exhibit low total acidity. Silanol groups contribute to weak and medium acidity [38,39], as observed in M0. The signal shift to higher temperatures or the increase of the type of acidity indi-

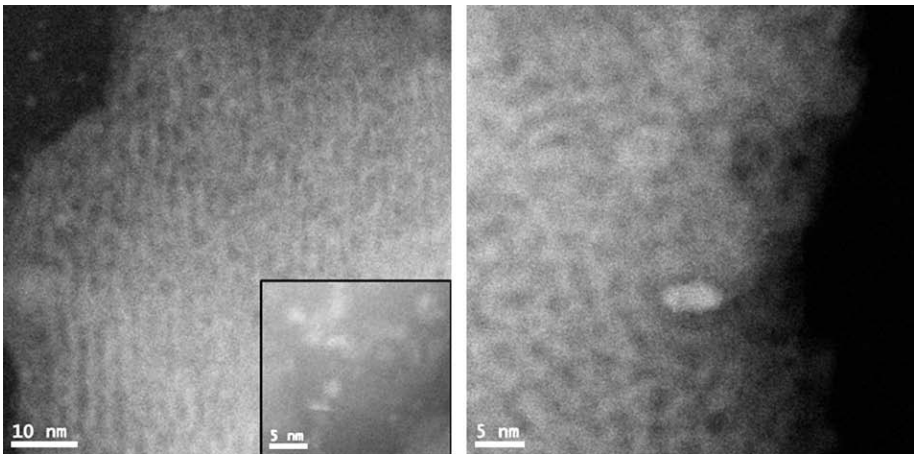

Fig. 4. TEM micrographs of SnMB25.

Table 2
Deconvoluted TPDA weak and medium strength signals of several Sn- and Zn-loaded MCM-41 materials.

Catalyst	Acidity, μmol desorbed ammonia/g catalyst			% Weak
	Weak	Medium	Total	
M0	10	8	18	25
SnMB16	2	38	40	3
SnMB25	32	35	67	40
SnMB7	5	42	47	7
SnMC113	53	60	113	40
SnMC68	60	109	169	31
SnMC129	58	91	149	34
SnMG195	59	26	85	56
SnMG94	66	44	110	47
ZnMC174	63	168	234	24
ZnMG340	135	248	383	32
ZnMG142	95	105	200	38

cates that the acidity of MCM-41 is increased by metal loading. The analyzed materials show weak and medium acid sites. The latter being the type of active sites reported for the Prins reaction [40,41]. UV–Vis and TPR analyses indicate the presence of Sn^{4+} as Lewis acid sites of different coordination [42] and SnO_2 nanoparticles [38]. Acidity measurements of SnO_2 suggest that Sn–OH species are weak acid sites. Meanwhile, different coordination states of Sn are responsible of medium and strong acid sites [43] and their distribution depends on heat treatment.

3.5. Fourier transform infrared spectroscopy

The FTIR spectra of adsorbed pyridine of several catalysts were obtained for the identification of acid sites (Fig. 6). The bands at 1596 and 1445 cm^{-1} have been assigned to pyridine weakly interacting with hydrogen bonds [44]. For MCM-41 these bands correspond to linked silanol groups and very weak acid free silanol species, respectively [45]. Additionally, the band at 1578 cm^{-1} has been attributed to Lewis acid sites due to superficial silanol groups [46]. Bands between 1485 and 1492 cm^{-1} assigned to both Bronsted and Lewis acid sites [47,48] are observed in the spectra of SnMG135, SnMC129 and ZnMG142. The presence of Lewis and Bronsted acid sites in SnMC129 and SnMG135 catalysts are suggested by the bands at 1614 cm^{-1} and near 1548 cm^{-1}, respectively [49]. Lewis acid sites of ZnMG142 and ZnMC118 are evidenced by the band around 1610 cm^{-1} [48].

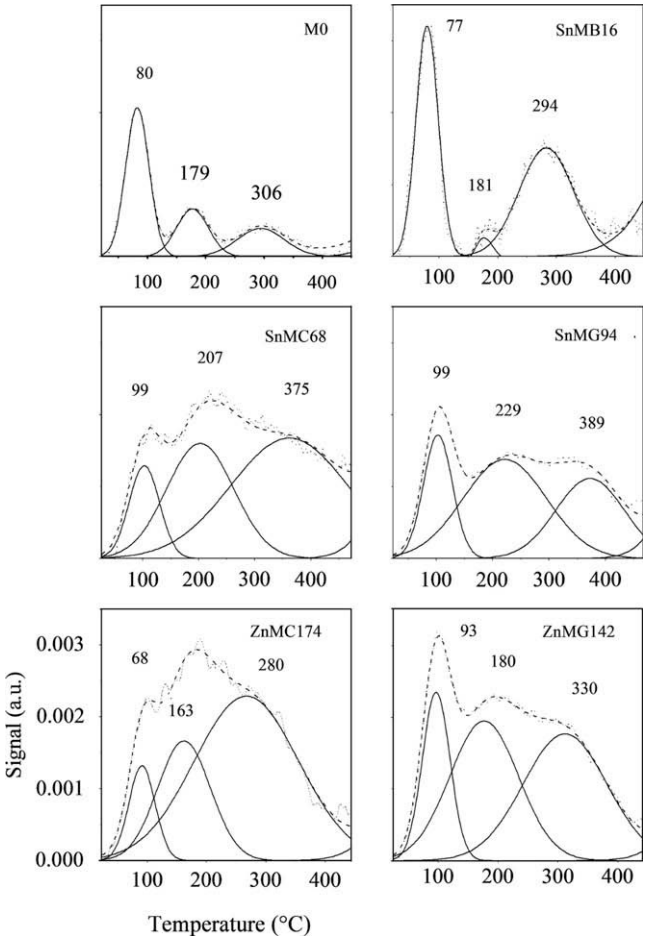

Fig. 5. Deconvoluted TPDA profile of selected Sn- and Zn-loaded MCM-41 materials. Inset values indicate the temperature of the corresponding fitted peak.

3.6. Catalytic tests

Table 3 shows the results of nopol production over several materials. Poor conversion is obtained over MCM-41 and materials with none or insignificant Sn loading (entries 5–7). We previously reported that the conversion and selectivity obtained over Sn–MCM-41 catalysts synthesized by CVD of $SnCl_4$ with metal loadings between 30 and 500 μmol Sn/g are similar [5]; however, current

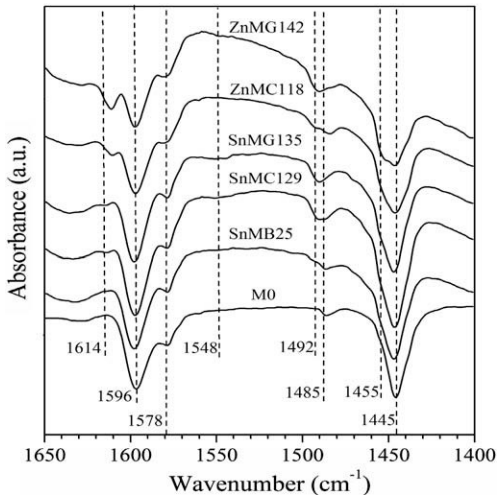

Fig. 6. FTIR spectra of adsorbed pyridine on several Sn- and Zn-loaded MCM-41 materials.

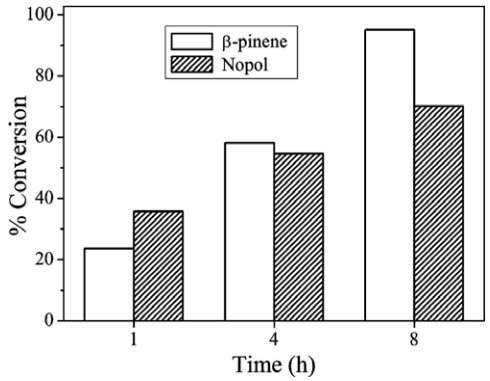

Fig. 7. Conversion of β-pinene and nopol on SnMB25, with no paraformaldehyde. Reaction conditions: 0.25 mmol substrate (β-pinene or nopol), 12.5 mg catalyst, 0.5 ml toluene, 80 °C.

results indicate that a metal loading around 16 μmol Sn/g gives a high yield. On the other hand, the selectivity of SnMB25 which is similar to M0 seems to be linked to the high proportion of weak acid sites. Although, a large amount of tin was deposited by CVD of $SnCl_2$ (entries 8–10), the TOF obtained with these materials is lower than on materials synthesized by CVD of $SnCl_4$ under static conditions (entries 2–4). It seems that the differences in the thermal treatment of Sn–MCM-41 materials synthesized by CVD could be responsible for the differences in acid site distribution. The highest selectivity was obtained over SnMB7 (entry 4) possessing a low total acidity and high proportion of medium acidity. SnMC195 and SnMG94 materials containing weak acid sites were less selective. SnMG*x* materials containing a high proportion of weak acid sites give high β-pinene conversion and low nopol selectivity (entries 13–15). Although, Zn–MCM-41 materials have larger amount of acid sites and metal loading than Sn–MCM-41 materials, β-pinene conversion and TOF were not appreciable. The low surface area of Zn-loaded materials may be another reason for their poor catalytic performance in nopol production. β-Pinene conversion, nopol selectivity and TOF were quite similar on ZnMG142 and ZnMC118 materials having strong Lewis acid sites; the same trend was observed over SnMC129 (entry 10) and SnMG135 (entry 14).

β-pinene and nopol conversions increased with time over SnMB25 in the absence of paraformaldehyde (Fig. 7). Under the reaction conditions of this study β-pinene and nopol may be isomerized [2,50] or polymerized [51]. The main by-product reported when nopol was obtained in homogeneous systems has been 4-(1-methyl etenyl)-1-cyclohexene-1-ethanol [50]. GC–MS analyses of reaction products over SnMB25, SnMC68 and SnMG94 yield camphene and limonene from isomerization of β-pinene and myrtenol from allylic oxidation reaction. Additionally, nopyl acetate from nopol was also obtained over SnMC68 and SnMB25, and bornyl formate over SnMC68. Only isomeric by-products as described above appear to be formed. Isomerization of α-pinene to camphene and limonene has been linked to weak and strong acid sites, respectively [52]. The formation of borneol type structure upon hydration of α-pinene was reported in an interesting review about the isomerization of pinenes over solid catalysts [53]. The broad distribution of acid sites in Sn–MCM-41 materials may be responsible for the differences in the type of by-products obtained.

Fig. 8 shows the results of leaching tests over SnMG94, SnMB25 and SnMC68. After removing the solid, conversion was negligible and close to the conversion obtained after 24 h in blank experiments. Without catalyst, β-pinene concentration in the reaction mixture did not vary more than 2% after 3, 6 and 24 h of additional reaction time. Summarizing, no leaching of the active species appears to occur during reaction over Sn–MCM-41 synthesized by different methods. Reusing of materials prepared by CVD of $SnCl_4$ [5] showed a progressive deactivation probably due to nopol remaining adsorbed on the catalyst after reaction. However, these materials can be activated by calcination.

From leaching tests (Fig. 8) and catalytic behavior (table 3) it can be inferred that β-pinene conversion decreased in the following order SnMG94 ≈ SnMB25 (98%) > SnMC68 (83%) > ZnMC118 (42%). β-pinene conversion over ZnMC118 is 8% after 24 h, under reaction conditions of Fig. 8. Furthermore, TOF decreased in the following order SnMB25 (392 h^{-1}) > SnMC68 (122 h^{-1}) > SnMG94 (105 h^{-1}). In agreement with previous studies over Sn–MCM-41 synthesized by CVD [54], selectivity may be improved by reducing catalyst amount, but in detriment of conversion. Results from table 3 and Fig. 8 show that nopol selectivity over SnMG94 can be modified by changing reaction conditions; nopol selectivity increased from 46% to 85% by decreasing catalyst amount.

Table 3
β-pinene conversion, nopol selectivity and TOF on Sn and Zn doped MCM-41[a].

Entry	Catalyst	Conversion (%)	Selectivity (%)	TOF (h^{-1})[b]
1	SnMB70[c]	91	83	130
2	SnMB16	95	79	594
3	SnMB25	98	73	392
4	SnMB7	70	84	1000
5	SnMB0	21	61	nd
6	SnMC0	7	57	nd
7	M0	8	71	nd
8	SnMC113	85	78	75
9	SnMC68	83	75	122
10	SnMC129	91	63	71
11	ZnMC174	56	73	32
12	ZnMC118	42	84	36
13	SnMG195	98	61	50
14	SnMG135	94	70	70
15	SnMG94	99	46	105
16	ZnMG340	58	82	17
17	ZnMG142	42	84	30

nd: Not determined.
[a] Reaction conditions: 0.25 mmol β-pinene, 0.5 mmol HCHO, 25 mg catalyst, 0.5 ml toluene, 90 °C, 1 h.
[b] Average turnover frequency for a 1 h-reaction.
[c] Catalyst Sn–MCM-41-D2 as cited in reference [5].

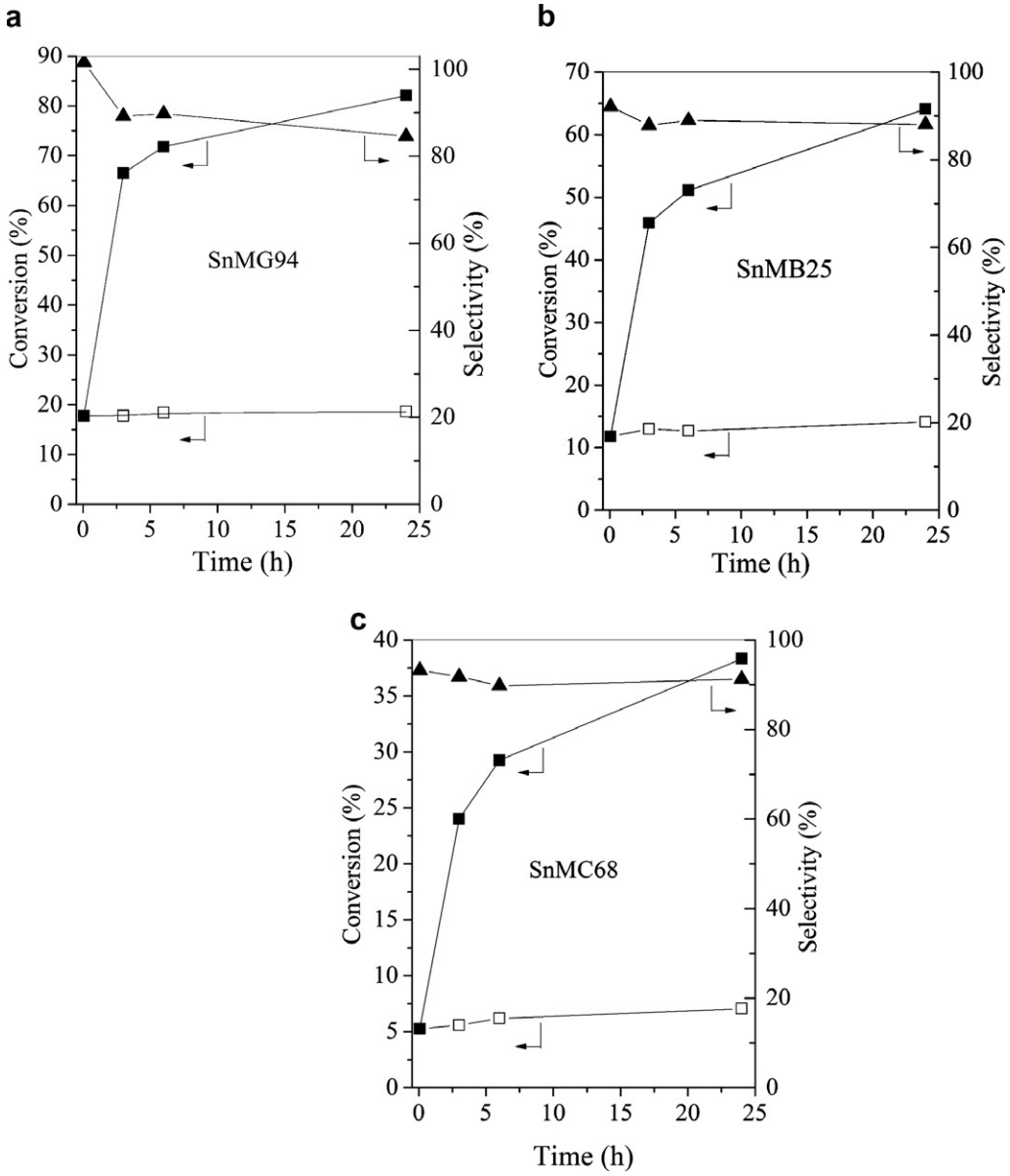

Fig. 8. Leaching tests of selected catalysts. Conversion and selectivity under current reaction conditions (filled symbols), after removing the solid after 5 min reaction and adding 0.9 mmol of HCHO (unfilled symbols). Reaction conditions: 1 ml of 0.5 M β-pinene in toluene, β-pinene to HCHO ratio of 1:2, 6 mg catalyst, 90 °C.

4. Conclusions

MCM-41 materials were modified with Sn and Zn by CVD and hydrothermal procedures. Higher β-pinene conversion and nopol selectivity are obtained over Sn–MCM-41 materials synthesized by CVD or hydrothermally than over Zn-loaded materials. Nopol selectivity over Sn–MCM-41 materials synthesized by CVD of either $SnCl_4$ or $SnCl_2$ as metal precursors is higher than that over hydrothermally synthesized Sn–MCM-41. All synthesized Sn–MCM-41 materials showed weak and medium acid sites, and Zn–MCM-41 materials exhibited higher amount of acid sites than Sn–MCM-41.

Acknowledgments

The authors are grateful to COLCIENCIAS and Universidad de Antioquia for sponsoring this work through the Excellence Center CENIVAM, Contract RC N°.432. E.A. acknowledges COLCIENCIAS his doctoral fellowship and Professor Amiridis Group at USC for TEM pictures.

References

[1] J.O. Bledsoe, in: J.I. Kroschwitz, M. Howe-Grant (Eds.), Kirk-Othmer Encyclopedia of Chemical Technology, vol. 23, Wiley, New York, 1997, p. 833.
[2] J.P. Bain, J. Am. Chem. Soc. 68 (1946) 638.
[3] Z. Wang, Z. Xiao, J. Chen, Jiangsu Chem. Ind. 33 (2005) 64.
[4] J.M. Ricca, P.J. Derian, J.P. Hecaen, J.M. Mercier, United States Patent No. 5674823, 1997.
[5] A.L. Villa de P., E. Alarcón, C. Montes de C., Catal. Today 107–108 (2005) 942.
[6] A. Corma, M. Renz, ARKIVOC 8 (2007) 40.
[7] M. Selvaraj, S. Kawi, J. Mol. Catal. A: Chem. 246 (2006) 218.
[8] U.R. Pillai, E. Sahle Demessie, Chem. Commun. (2004) 826.
[9] R. Ryoo, S. Jun, J.M. Kim, M.J. Kim, Chem. Commun. (1997) 2225.
[10] H.Y. Zhang, Y.J. He, Y.B. Chen, H.Y. Wang, J. Appl. Phys. 92 (2002) 7636.
[11] S. Nishiyama, M. Yamamoto, H. Izumida, S. Tsuruya, J. Chem. Eng. Jpn. 37 (2004) 310.

[12] M. Grün, K.K. Unger, A. Matsumoto, K. Tsusumi, Micropor. Mesopor. Mater. 27 (1999) 207.
[13] N. Nishiyama, M. Yamaguchi, Y. Nishiyama, Y. Egashira, K. Ueyama, J. Non-Cryst. Solids 351 (2005) 3218.
[14] M. Stockenhuber, R.W. Joyner, J.M. Dixona, M.J. Hudson, G. Grubert, Micropor. Mesopor. Mater. 44–45 (2001) 367.
[15] A.L. Villa, Epoxidation of Monoterpenes by Homogeneous and Heterogeneous Catalytic Systems, Katholieke Universiteit Leuven, 2000, pp. 30–35.
[16] S. Jiang, Y. Kong, J. Wang, X. Ren, Q. Yan, J. Porous Mater. 13 (2006) 341.
[17] X.S. Zhao, G.Q. Lu, A.K. Whittaker, G.J. Millar, H.Y. Zhu, J. Phys. Chem. B 101 (1997) 6525.
[18] R. Savidha, A. Pandurangan, Appl. Catal. A Gen. 276 (2004) 39.
[19] K. Chaudhari, T.K. Das, P.R. Rajmohanan, K. Lazar, S. Sivasanker, A.J. Chandwadkar, J. Catal. 183 (1999) 281.
[20] S. Kowalak, K. Stawinski, A. Makowiak, Micropor. Mesopor. Mater. 44–45 (2001) 283.
[21] T. Burch, V. Caps, D. Gleeson, S. Nishiyama, S.C. Tsang, Appl. Catal. A Gen. 194 (2000) 297.
[22] P.W. Park, H.H. Kung, D.W. Kim, M.C. Kung, J. Catal. 184 (1999) 440.
[23] S.W. Park, O.S. Joo, K.D. Jung, H. Kim, S.H. Han, Appl. Catal. A Gen. 211 (2001) 81.
[24] Y. Wang, C. Ma, X. Sun, H. Li, Mater. Lett. 51 (2001) 285.
[25] N.N. Greenwood, A. Earnshaw, Chemistry of the Elements, Butterworth-Heineman, Great Britain, 1997. (pp. 382–385).
[26] M.N. Rumyantseva, A.M. Gaskov, N. Rosman, T. Pagnier, J.R. Morante, Chem. Mater. 17 (2005) 893.
[27] T.F. Kuznetsova, Inorg. Mater. 38 (2002) 1015.
[28] A. Corma, T. Navarro, M. Renz, J. Catal. 219 (2003) 242.
[29] Y. Teraoka, S. Ishida, A. Yamasaki, N. Tomonaga, A. Yasutake, J. Izumi, I. Moriguchi, S. Kawaga, Micropor. Mesopor. Mater. 48 (2001) 151.
[30] T.R. Gaydhankar, P.N. Joshi, P. Kalita, R. Kumar, J. Mol. Catal. A: Chem. 265 (2007) 306.
[31] M. Wark, Y. Rohlfing, Y. Altindag, H. Wellmann, Phys. Chem. Chem. Phys. 5 (2003) 5188.
[32] L. Wang, S. Sang, S. Meng, Y. Zhang, Y. Qi, Z. Liu, Mater. Lett. 61 (2007) 1675.
[33] W.H. Zhang, J.L. Shi, L.Z. Wang, D.S. Yan, Chem. Mater. 12 (2000) 1408.
[34] S.G. Hur, T.W. Kim, S.J. Hwang, S.H. Hwang, J.H. Yang, J.H. Choy, J. Phys. Chem. B 110 (2006) 1599.
[35] S. Wang, X. Ma, J. Gong, X. Yang, H. Guo, G. Xu, Ind. Eng. Chem. Res. 43 (2004) 4027.
[36] F. Arena, R. Dario, A. Parmaliana, Appl. Catal. A Gen. 170 (1998) 127.
[37] M. Niwa, N. Katada, M. Sawa, Y. Murakami, J. Phys. Chem. 99 (1995) 8812.
[38] P. Shah, A.V. Ramaswamy, K. Lazar, V. Ramaswamy, Appl. Catal. A Gen. 273 (2004) 239.
[39] A. Jentys, K. Kleestorfer, H. Vinek, Micropor. Mesopor. Mater. 27 (1999) 321.
[40] E. Dumitriu, V. Hulea, L. Fechete, C. Catrinescu, A. Auroux, J.F. Lacaze, C. Guimon, Appl. Catal. A Gen. 181 (1999) 15.
[41] E. Dumitriu, D. Trong On, S. Kaliaguine, J. Catal. 170 (1997) 150.
[42] M. Rumyantseva, V. Kovalenko, A. Gaskov, E. Makshina, V. Yuschenko, I. Ivanova, A. Ponzoni, G. Faglia, E. Comino, Sensor. Actuat. B Chem. 118 (2006) 208.
[43] V.V. Kovalenko, A.A. Zhukova, M.N. Rumyantseva, A.M. Gaskov, V.V. Yushchenko, I.I. Ivanova, T. Pagnier, Sensor. Actuat. B Chem. 126 (2007) 52.
[44] B. Chakraborty, B. Viswanathan, Catal. Today 49 (1999) 253.
[45] A. Ramírez, B.L. Lopez, L. Sierra, J. Phys. Chem. B 107 (2003) 9275.
[46] M. Casagrande, L. Storaro, M. Lenarda, J. Gersich, L. Stievano, F.E. Wagner, T. Montanari, J. Mater. Chem. 14 (2004) 1010.
[47] M. Mohamed, Spectrochim. Acta 51A (1995) 1.
[48] G.A. Eimer, S.G. Casuscelli, C.M. Chanquia, V. Elías, M.E. Crivello, E.R. Herrero, Catal. Today 133–135 (2008) 639.
[49] G. Busca, Phys. Chem. Chem. Phys. 1 (1999) 723.
[50] Z. Xiao, Z. Li, J. Chen, Y. Fu, M. Wang, J. Jiangxi Norm, Univ. Nat. Sci. Ed. 23 (1999) 360.
[51] C. Gonzebach, M. Jordan, R. Yunick, in: H.F. Mark, N.G. Gaylord, N.M. Bikales (Eds.), Encyclopedia of Polymer Science and Technology Plastics Resins Rubbers Fibers, vol. 13, John Wiley and sons, USA, 1964, p. 575.
[52] N.A. Comelli, E.N. Ponzi, M.I. Ponzi, Chem. Eng. J. 117 (2006) 93.
[53] K.A.D. Swift, in: R.A. Sheldon, H. van Bekkum (Eds.), Fine Chemicals through Heterogeneous Catalysis, Wiley-VCH, Weinheim, 2001, p. 242.
[54] E. Alarcón, A.L. Villa de P., C. Montes de C., Rev. Fac. Ing. Univ. Antioquia 36 (2006) 42.